Preprint Dated: June 15, 1999, at 10:36
Submitted to: *Plasma Physics and Controlled Fusion*

The Mercier Criterion in Reversed Shear Tokamak Plasmas

M. S. Chance, C. Kessel and S. C. Jardin

Princeton University Plasma Physics Laboratory
P.O. Box 451, Princeton, NJ 08543, USA

June 15, 1999

Abstract

A recent numerical study has found that, contrary to conventional theoretical and experimental expectations, reversed shear plasmas are unstable primarily because the term proportional to the shear in the Mercier criterion is destabilizing. In the present study, the role of the magnetic shear, both local and global, is examined for various tokamak configurations with monotonic and non-monotonic safety factor profiles. The enhancement of the local shear due to the outward shift of the magnetic axis suggests that the latter are less susceptible to interchanges. Furthermore, by regrouping the terms in the criterion, the V'' term when differentiated instead with respect to the *toroidal* flux, is shown to absorb the dominant shear term. No Mercier instability is found for similar profiles as in the previous study.

PACS: 52.35.Py, 52.55.Fa

1 Introduction

A recent study[1] has found that the Mercier criterion[2, 3, 4] was violated in the inner region of a reversed shear plasma. It found that the instability occurred when the safety factor on axis, $q_{\rm axis}$, exceeded a threshold, for fixed value of the minimum, $q_{\rm min}$, location of the minimum, $r_{\rm min}$, the edge value of the safety factor, $q_{\rm edge}$, and for fixed pressure profile. In addition, the region of instability was found to be where the magnetic shear, $q'(\psi)$, is negative. This has contradicted the generally established notion that negative shear is robustly Mercier and balloon stable, both from semi-analytical results[5] and favorable numerical[6] and experimental[7, 8] evidence from several tokamak devices. Since the reversed shear configuration has become a premier option for a high performance tokamak reactor[9, 10], we have attempted to corroborate the results of Ref. [1]. Analytical calculations of the Mercier criterion can be done only for simple limits, e.g., in the vicinity of the magnetic axis, but nevertheless we present convincing evidence that the general configurations studied are robustly stable.

For pressure profiles similar to those in Ref. [1], in a fixed boundary circular cross-section plasma, we have found no Mercier instability for a representative range of $q(\psi)$

with negative shear. We have also examined plasmas with the ITER reversed shear plasma shape (with elongation $\kappa = 2.0$, and triangularity $\delta = 0.5$) and found no Mercier instability. We can however get instability in the core region for reversed D-shaped configurations. In order to understand this behavior more fully, we have regrouped the terms in the Mercier criterion to elucidate the role which the shear term plays in determining the stability of the configurations studied. It is found that the quantity V^{tt}, i.e., the second derivative of the plasma volume within a flux surface with respect to the *toroidal*, rather than with respect to the *poloidal* flux, V'', is more suitable for inclusion in the criterion, since the dominant shear term is absorbed in V^{tt}. We also show that the modification of the local magnetic shear properties due to the shift of the magnetic axis is significantly different between non-reversed and reversed configurations, giving further evidence that stability is more favored in the latter cases.

The next section of this paper, Sec. 2, describes the basic equations and our notations and normalizations, etc. Sec. 3 describes configuration of the circular cross section plasma studied. The terms in Mercier criterion are regrouped to best illustrate the role of shear in determining stability features. Results from monotonic $q(\psi)$ and non-circular cross-section plasmas are described. Sec. 4 describes stability calculations done in non-circular cross sections. Significant differences in the local magnetic shear structure between reversed and non-reversed shear plasmas are illustrated in Sec. 5. Next, in Sec. 6, some speculative reasons for the discrepancy between Ref. [1] and our study. Finally, concluding remarks and acknowledgments are presented in the last sections, Secs. 7 and 8.

2 Preliminaries

Denoting the equilibrium current density, magnetic field and pressure respectively by $\mathbf{J}$, $\mathbf{B}$ and p, in rationalized Gaussian units with the speed of light, c = 1, the MHD system of equations relevant to this work are:

$$\mathbf{J} \times \mathbf{B} \quad = \quad \nabla p, \tag{1}$$

with

$$\mathbf{J} \quad = \quad \nabla \times \mathbf{B}. \tag{2}$$

The tokamak magnetic field is written as

$$\mathbf{B} \quad = \quad \nabla\phi \times \nabla\psi + g(\psi)\nabla\phi, \tag{3}$$

so that the poloidal magnetic flux, Ψ, is $2\pi\psi$ within the volume, V, and $g(\psi)(= 2\pi R B_\phi)$ is the toroidal field function. For operational purposes, the beta of the plasma is defined in terms of MKS units and is given by: $\beta \equiv 2\mu_0\langle p\rangle_{\rm v}/B_0^2 \equiv \beta_N(I_p/aB_0)$ where the pressure is given in Newton/meters^2, the toroidal plasma current I_p is in units of mega-amperes, the minor radius a in meters measured from the geometrical center at $R = R_0$, and the vacuum toroidal magnetic field strength B_0 at the geometric center of the plasma in tesla. $\langle\cdots\rangle_{\rm v}$ denotes the volume average. With these definitions the poloidal beta, $\beta_{\rm pol}$, is $2\mu_0\langle p\rangle_{\rm v}/B_p^2$, with

$$B_p \quad \equiv \quad \frac{\mu_0 I_p}{2\pi a\sqrt{(1+\kappa^2)/2}}, \tag{4}$$

where κ is the elongation of the plasma. The coordinate system used is such that $\mathbf{r} = (R, \phi, Z) = (\psi, \theta, \phi)$, with the Jacobian, $\mathcal{J} = (\nabla\psi \times \nabla\theta \cdot \nabla\phi)^{-1}$ The plasma surface is parameterized as

$$X = R_0 + a\cos(\theta + \delta\sin\theta), \tag{5}$$

$$Z = \kappa\, a \sin\theta, \tag{6}$$

where the elongation, κ, and the triangularity, δ, are defined by Eqs. (5) and (6).

Instead of the conventional normalized averages over the poloidal angle, θ, these are defined as:

$$\langle \cdots \rangle \equiv \frac{1}{2\pi} \oint \cdots d\theta. \tag{7}$$

Then, with $' \equiv \partial/\partial\psi$,

$$V' = 4\pi^2 \langle \mathcal{J} \rangle, \tag{8}$$

and the safety factor, $q(\psi)$, is

$$q = \frac{\partial\Phi}{\partial\Psi} = g\left\langle \frac{\mathcal{J}}{R^2} \right\rangle, \tag{9}$$

where Φ is the toroidal flux. The integrals are evaluated numerically using the trapeziodal rule because of the extremely high accuracy offered by the Euler-Maclaurin effect[11] for periodic functions. Less accurate methods have proved to be inadequate when analyzing advanced tokamak configurations. High accuracy is necessary since the Mercier criterion often results from the cancellations of individually large terms.

Pertinent to the later discussion involving the local magnetic shear, $S(\psi, \theta)$, the latter is defined as,[4, 5, 12]

$$S(\psi, \theta) = -\frac{\mathbf{B} \times \nabla\psi}{|\nabla\psi|^2} \cdot \nabla \times \frac{\mathbf{B} \times \nabla\psi}{|\nabla\psi|^2}, \tag{10}$$

and can be written in the form,

$$S(\psi, \theta) = \frac{1}{\mathcal{J}} \left[\left(\frac{\mathcal{J} g}{R^2} \right)' + \frac{\partial}{\partial\theta} \left(\frac{\nabla\psi \cdot \nabla\theta}{|\nabla\psi|^2} \frac{\mathcal{J} g}{R^2} \right) \right]; \tag{11}$$

since

$$\langle \mathcal{J} S(\psi, \theta) \rangle = q'(\psi), \tag{12}$$

we see that $S(\psi, \theta)$ is comprised of the averaged global shear, $q'(\psi)$ and a residual oscillating part which vanishes under the averaging. A normalized S is defined such that

$$\hat{S} \equiv \frac{V}{2\pi^2 q} S; \tag{13}$$

then,

$$\frac{\left\langle \mathcal{J} \hat{S}(\psi, \theta) \right\rangle}{\langle \mathcal{J} \rangle} = 2 \frac{V}{V'} \frac{q'}{q}. \tag{14}$$

For the numerical simulations, the Mercier criterion as well as the infinite toroidal mode number (n) ballooning mode criterion were examined for both circular and ITER-like reversed shear steady state configurations. In order that these results are well documented and reproducible, essential details about the configurations studied and the methods used are presented here.

The functional form of the pressure profile used in this study is

$$p(\psi) = p_o(1 - \hat{\psi}^{\beta_p})^{\alpha_p}, \tag{15}$$

where the values for (α_p, β_p) are fixed at (2.00,1.00) in order to correspond to the profiles of Ref. [1]. The functional form for the parallel current density profiles is given by,

$$\frac{\langle \mathcal{J}\mathbf{J}\cdot\mathbf{B}\rangle}{\langle \mathcal{J}\mathbf{B}\cdot\nabla\phi\rangle}(\psi) = j_o(1-\hat{\psi}^{b_j})^{a_j} + j_1\frac{d^2\hat{\psi}^{\alpha_j}(1-\hat{\psi})^{\beta_j}}{(\hat{\psi}-\psi_o)^2+d^2}. \tag{16}$$

Here, $\hat{\psi} \equiv (\psi - \psi_{\rm axis})/(\psi_{\rm edge} - \psi_{\rm axis})$, and the coefficients j_o and j_1 respectively provide profile shaping for on-axis peaking, and off-axis peaking at ψ_o with width parameter d.

The equilibria are produced with the fixed boundary flux coordinate equilibrium code JSOLVER, using 257 poloidal flux surfaces and 512 poloidal angle points in 2π. The Mercier and n=∞ ballooning stability analyses are done with the code BALMSC.

The curves generated in this study by data values f are plotted using a *modified* hyperbolic sine *scale*, $\sinh_{10}$ say, defined as follows:

$$f = \frac{10^y - 10^{-y}}{\gamma} = \frac{2}{\gamma}\sinh(y\log_{\rm e}10), \tag{17}$$

$$\equiv \frac{2}{\gamma}\sinh_{10}(y) \tag{18}$$

with the inverse,

$$y = \sinh_{10}^{-1}(\gamma f) \tag{19}$$

$$= \log_{10}\left(\frac{\gamma f}{2} + \sqrt{\left(\frac{\gamma f}{2}\right)^2 + 1}\right), \tag{20}$$

$$= -\log_{10}\left(-\frac{\gamma f}{2} + \sqrt{\left(\frac{\gamma f}{2}\right)^2 + 1}\right), \tag{21}$$

where the latter form for y is numerically more suitable when γf is negative. For $|y| \gtrsim 1$ the scale rapidly approaches the usual logarithmic scale, i.e., $y = \mathrm{sign}(\gamma f)\log_{10}|\gamma f|$, for both positive and negative values. On the other hand, for $\gamma f \ll 1$, $f \sim (2y/\gamma)\log_{\rm e}10$, so by setting $\gamma = 2\log_{\rm e}10$, one can have $f \sim y$ for small f. Other values of γ can be a stretching or contraction factor effective at small y.

This scale allows plotting data which smoothly span large and small values of either sign. This is particularly useful in the present study since, as mentioned above, D_I is often comprised of the residual of large terms of opposite signs, and we wish to display plots of these terms together in a single figure. In this study γ is fixed at 10 so that for $|y| \gtrsim 1$, $y \sim 1 + \log_{10} f$. A similar scale was used to display the properties of the full MHD spectrum in an unstable plasma.[13]

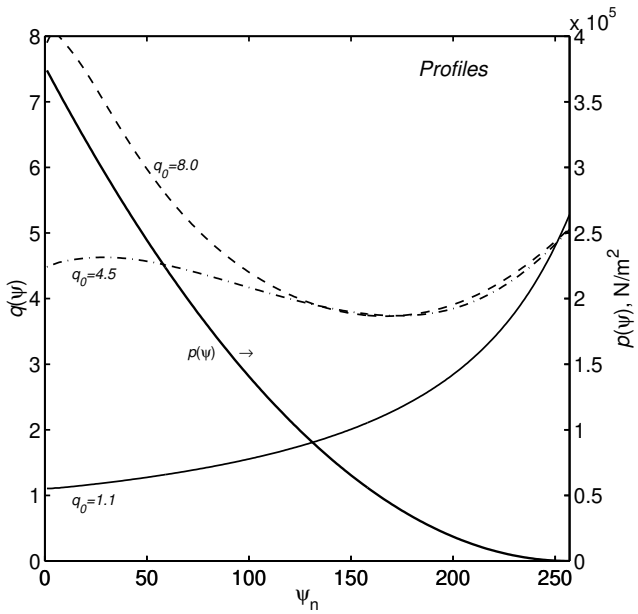

Figure 1: Safety factor profiles (lighter lines) for the reversed shear cases, $q_{\rm axis} = 4.5$ and 8.0, and the monotonic case for which $q_{\rm axis} = 1.1$. The pressure profile shown with the heavier line is the same for all cases.

3 Circular configurations

We investigated a variety of reversed shear configurations similar to the circular case of Ref. [1], using representative values of $q_{\rm axis}$ of 4.5 and 8.0, holding $q_{\rm min}$, $r_{\rm min}$ and $q_{\rm edge}$ approximately fixed. With the magnetic axis at $R = 9$, and a minor radius, a, of 3 the aspect ratio is fixed at 3.0. For the parallel current density profile the parameters (a_j, b_j, d, α_j, β_j, ψ_o) of Eq. (16) are given by (1.0, 1.0, 0.3, 1.0, 2.0, 0.8) for $q_{\rm axis} = 4.5$, and (1.0, 1.0, 0.4, 1.0, 2.0, 0.7) for $q_{\rm axis} = 8.0$. The corresponding values of (j_o, j_1) are $(1.526 \times 10^6, 3.181 \times 10^7)$ and $(9.125 \times 10^5, 2.763 \times 10^7)$. β_N values lying within the range (1.5–4.0) corresponding to a range of $\beta_{\rm pol}$ of (1.1–3.0) were analyzed. For completeness we also studied a non-reversed shear case with $q_{\rm axis} = 1.1$. For this case we used $(a_j, b_j, j_o, j_1) = (1.5, 1.1, 6.237 \times 10^6, 0.0)$.

The safety factor profiles for the $\beta_N = 2.0$ case with $q_{\rm axis}$ equal to 1.1, 4.5 and 8.0 are shown as a function of the poloidal flux surface number in Fig. 1 together with the pressure profile which is used for all the cases studied. Note that the pressure gradient is generally largest in the reversed shear region. The safety factor profile for the case where $q_{\rm axis} = 4.5$ has a slight local maximum near the origin. As detailed below, no Mercier instabilities are observed in these cases. The n=∞ ballooning instability appears only for the $q_{\rm axis} = 8.0$ case at the highest β_N and occurs in the traditional location for reverse shear plasmas, where the magnetic shear begins to rise outside the $q_{\rm min}$ location.

The plasma volume within a flux surface for these configurations is plotted as a function of the poloidal flux surface number in Fig. 2(left). The curvature, V'', of the lines tends to be positive (negative) in the positive (reversed) shear region. The dotted line is straight. On the right are curves of the major radius along the midplane as a function of the poloidal flux. These can be used to map the flux surfaces onto configuration space.

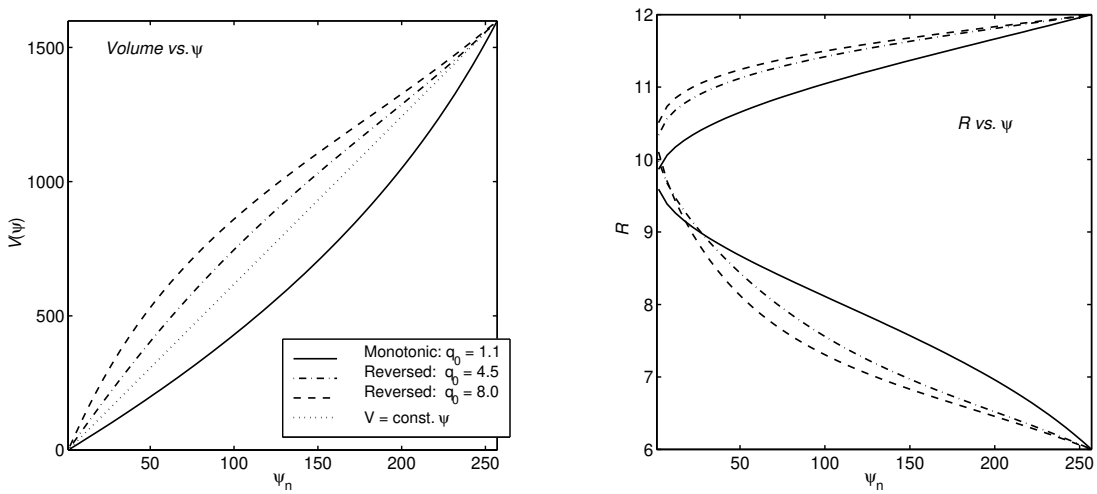

Figure 2: On the left: the plasma volume, V, as a function of the poloidal flux number for monotonic and reversed shear safety factor profiles. The curvature, V'', of the lines tends to be positive (negative) in the positive (reversed) shear region. The dotted line is straight. On the right is shown the mapping of the flux surface number to the major radius along $Z = 0$. The magnetic axes are shifted from the geometrical center at $R = R_0 = 9$.

3.1 The Mercier criterion

The form of the Mercier criterion with the terms grouped similarly to those given in Ref. [1], but using our notation and normalization described in Sec. 2 is:

$$\begin{aligned} q'^2 D_I &= -\frac{q'^2}{4} \\ &+ \left[\left\langle \frac{\mathcal{J}B^2}{|\nabla\psi|^2} \right\rangle \left\langle \sigma^2 \frac{\mathcal{J}B^2}{|\nabla\psi|^2} \right\rangle - \left\langle \sigma \frac{\mathcal{J}B^2}{|\nabla\psi|^2} \right\rangle^2 \right] \\ &- q' \left[\left\langle \sigma \frac{\mathcal{J}B^2}{|\nabla\psi|^2} \right\rangle + g' \left\langle \frac{\mathcal{J}B^2}{|\nabla\psi|^2} \right\rangle \right] \\ &- \left\langle \frac{\mathcal{J}B^2}{|\nabla\psi|^2} \right\rangle \left[p' \frac{V''}{4\pi^2} - p'^2 \left\langle \frac{\mathcal{J}}{B^2} \right\rangle \right], \end{aligned} \tag{22}$$

where $q'^2 D_I \leq 0$ for stability. Here, q' denotes the global magnetic shear, and the parallel current, $\sigma \equiv \mathbf{J} \cdot \mathbf{B}/B^2 = -gp'/B^2 - g'$.

The groups of terms comprising Eq. (22) are plotted in Fig. 3a for the case where $q_{\text{axis}} = 4.5$. Considering the right hand side, the negative definite first term, labeled by 's^2' in the figure, is stabilizing, and, because of the *Schwartz inequality*, the second group of terms, labeled 'scz' is always destabilizing (in the cylindrical limit this vanishes but contributes significantly to D_I in realistic configurations). Note that, because of it's structure any expression in σ independent of θ, i.e., $g'(\psi)$, cancels and then it can be written as,

$$+ g^2 p'^2 \left[\left\langle \frac{\mathcal{J}B^2}{|\nabla\psi|^2} \right\rangle \left\langle \frac{\mathcal{J}}{B^2|\nabla\psi|^2} \right\rangle - \left\langle \frac{\mathcal{J}}{|\nabla\psi|^2} \right\rangle^2 \right]. \tag{23}$$

A similar cancellation occurs in the third group of terms, labeled 'shear', which then be-

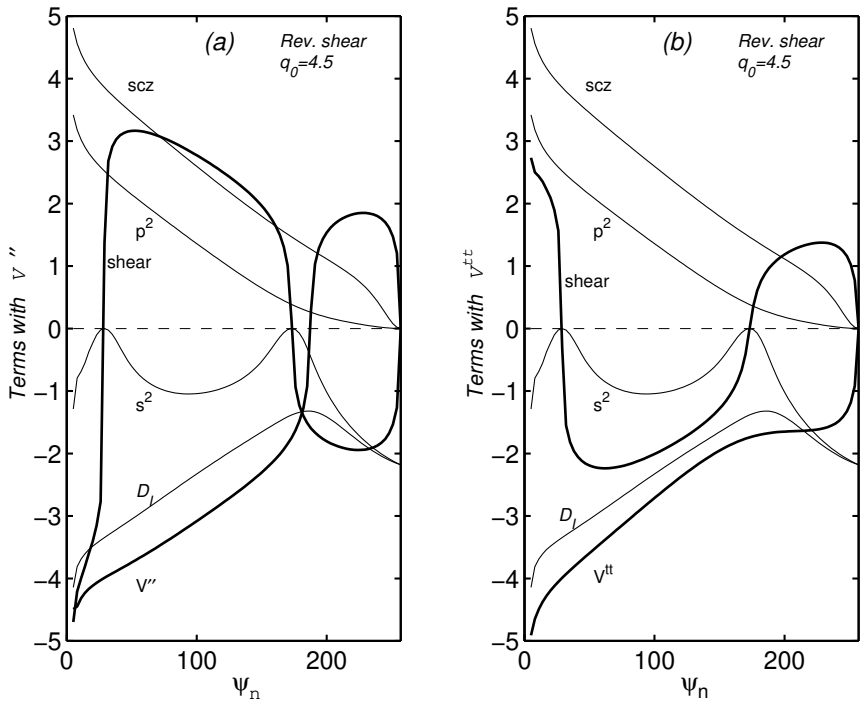

Figure 3: The terms of D_I using V'' (a), and V^{tt} (b), for a reversed shear profile. $q_{\rm axis} = 4.5$. The heavier curves of V'' and the shear term labeled "shear" in (a) combine to give the curves of V^{tt} and the shear term labeled "shear" in (b). The scale is the *modified* hyperbolic sine *scale*, $\sinh_{10}$, described in the text.

comes:

$$+ gq'p' \left\langle \frac{\mathcal{J}}{|\nabla\psi|^2} \right\rangle ; \tag{24}$$

this is the so called "shear" term and as pointed out in [1] it is destabilizing (stabilizing) for q' negative (positive), since g is positive and p' is negative. It was considered by [1] to be the dominant cause for the instability of reversed shear configurations. The role of magnetic shear will be more fully discussed in Sec. 5. In the fourth group of terms, labeled 'V''' in the figure, the less dominant term with p'^2 is destabilizing. The expression involving $V''(= \partial^2 V/\partial\psi^2)$, the "well" term, is by far the more dominant one in the cases studied and is found to be *stabilizing* in regions where the global shear is negative, but *destabilizing* in regions of positive shear. This is consistent with the behavior of the volume profiles shown in Fig. 2, but this counterintuitive change in the sign of V'' within the cross-section of the plasma suggests that it is not a good indication of the stabilizing tokamak magnetic well. The curves in the figure representing V'' and the "shear" terms are emphasized with the darker lines. Note that D_I, labeled 'D_I' is negative, (i.e. stable) over the whole plasma.

3.2 The Mercier criterion with V^{tt}

In order to understand the role that global shear plays in the stability criterion we make a judicious rearrangement of the terms which comprises D_I. An examination of Fig. 3a shows that the value of the shear term is approximately equal and opposite to that of the

"well" term. This suggests that a more appropriate use of V (albeit roughly) for describing the tokamak magnetic well is $V^{tt}(\equiv \partial^2 V/\partial\Phi^2)$, where Φ is the *toroidal* flux [on average, magnetic field lines circulate q times around the long way of the torus before making it once around the short way]. We can thus write,

$$V'' = 4\pi^2 q^2 V^{tt} + \frac{q'}{q}V'; \tag{25}$$

the term involving q', a "shear" term, is largely responsible for the change of sign in V''. It will oppose the dominant (toroidal) contribution of the shear term of Eq. (22) or (24). Substituting Eq. (25) and combining the shear terms, the Mercier criterion then takes the form:

$$\begin{aligned} q'^2 D_I = & -\frac{q'^2}{4} \\ & + g^2 p'^2 \left[\left\langle \frac{\mathcal{J} B^2}{|\nabla\psi|^2} \right\rangle \left\langle \frac{\mathcal{J}}{B^2 |\nabla\psi|^2} \right\rangle - \left\langle \frac{\mathcal{J}}{|\nabla\psi|^2} \right\rangle^2 \right] \\ & - \frac{q'p'}{q} \left[\left\langle \mathcal{J} \right\rangle \left\langle \frac{\mathcal{J} B^2}{|\nabla\psi|^2} \right\rangle - \left\langle \mathcal{J} B^2 \right\rangle \left\langle \frac{\mathcal{J}}{|\nabla\psi|^2} \right\rangle \right] \\ & - \frac{q'p'}{q} \left\langle \frac{\mathcal{J}|\nabla\psi|^2}{R^2} \right\rangle \left\langle \frac{\mathcal{J}}{|\nabla\psi|^2} \right\rangle \\ & - \left\langle \frac{\mathcal{J} B^2}{|\nabla\psi|^2} \right\rangle \left[p' q^2 V^{tt} - p'^2 \left\langle \frac{\mathcal{J}}{B^2} \right\rangle \right], \end{aligned} \tag{26}$$

where $q'^2 D_I \leq 0$ for stability.

The groups of these terms are plotted in Fig. 3b for the same configuration as was used for Fig. 3a. The residuals from the shear terms, i.e., the third and fourth groups on the right, plotted together and labeled 'shear' in the figure, are now reduced to the poloidal field scale; in the cylindrical limit the former now also vanish. In the reversed shear cases studied, these residuals are both stabilizing in the negative shear region. This is obviously true of the fourth group. A heuristic calculation of the third group of terms can substantiate its behavior as follows:

Assuming $B^2 \sim 1 - 2\varepsilon\cos\theta$, $|\nabla\psi|^{-2} \sim 1 - \Delta\cos\theta$, and $\mathcal{J} \sim 1 + \tau\cos\theta$, with ε, Δ and $\tau \ll 1$, the third group of terms becomes $\sim -(p'q'/q)\varepsilon\Delta(1 - \tau^2/2)$. If the magnetic field decreases with distance from the major axis ($\varepsilon > 0$) and if there is outward shifting of the magnetic surfaces ($\Delta > 0$), this group is stabilizing for negative shear (with p' negative); this is independent of $\mathcal{J}$ to leading order. These residuals can also be written as

$$\begin{aligned} & -\frac{q'p'}{q} g^2 \left[\left\langle \mathcal{J} \right\rangle \left\langle \frac{\mathcal{J}}{R^2 |\nabla\psi|^2} \right\rangle - \left\langle \frac{\mathcal{J}}{R^2} \right\rangle \left\langle \frac{\mathcal{J}}{|\nabla\psi|^2} \right\rangle \right] \\ & \qquad - \frac{q'p'}{q} \left\langle \mathcal{J} \right\rangle \left\langle \frac{\mathcal{J}}{R^2} \right\rangle, \end{aligned} \tag{27}$$

which gives a similar heuristic result but with the plasma diamagnetism term, g^2, extracted in this case.

The "well" term containing V^{tt}, labeled 'V^{tt}', is now negative throughout the plasma cross-section for all the positive and reversed shear cases studied. This is more appropriate

to describe the intrinsic property of tokamak wells. It is this form which tends to $\sim (1-q_0^2)$ at the magnetic axis.[3]

In the cylindrical limit we have also,[3]

$$V^{tt} \rightarrow \frac{R_0}{rB_z^4}\left[\frac{B_\theta}{r}\frac{\partial}{\partial r}(rB_\theta)+\frac{\partial p}{\partial r}\right], \tag{28}$$

$$\equiv V_{0c}^{tt}+\frac{R_0}{rB_z^4}\frac{\partial p}{\partial r}. \tag{29}$$

A sufficient condition for the cylindrical pinch to be stable to all fixed boundary MHD modes is that the dominant term, $V_{0c}^{tt} \leq 0$.[14]

There is a further cancellation of the pressure contributions in the " well" term of Eq. (26) and that in Eq. (29) so that,

$$q^2V^{tt}-p'\left\langle\frac{\mathcal{J}}{B^2}\right\rangle \rightarrow q^2V_{0c}^{tt}+\frac{r}{R_0B_z^2B^2}\frac{\partial p}{\partial r}, \tag{30}$$

where the second term is now very small and negative, thus making the overall "well" term stabilizing if V_{0c}^{tt} is negative.

Note that V^{tt} is still not a strictly reliable criterion for stability is evidenced by the fact that in a reversed-D configuration that we examined, V^{tt} is still negative although D_I is positive near the origin. This is of course necessary to compensate for the *Schwartz* and other destabilizing terms.

Similar results are found when the configuration with $q_{\text{axis}} = 8.0$ is examined. These are shown in Fig. 4. The safety factor profile lacks the local extremum near the origin in this case.

3.3 Monotonic $q(\psi)$ profile

The terms of D_I given by Eq. (22) for the circular configuration with a monotonic $q(\psi)$ profile in is shown in Fig. 5a. Although D_I is negative throughout the cross section we see again that the destabilizing "well" term is now opposed by the shear term which is now stabilizing. When the terms are grouped with V^{tt} according to Eq. (26) we see from Fig. 5b that the shear term is destabilizing but V^{tt} is negative throughout the cross section.

Note that there is approximately an order of magnitude cancellation between the large "well" and shear terms in the two forms of D_I, in configurations with either reversed or monotonic shear profiles.

4 Non-circular plasmas

In addition to the circular plasma cases analyzed above, for thoroughness we have also examined plasmas with the ITER reversed shear plasma shape ($\kappa = 2.0$, $\delta = 0.5$) and found no Mercier instability for q_{axis} ranging from 4.5 to 10.0.

The plasma boundary is taken from the Reversed Shear discharge simulation performed with the Tokamak Simulation Code (TSC). The q_{axis} value is increased from 4.5 to 6.0, 8.0, and 10.0, holding the q_{min}, r_{min}, q_{edge} and the pressure profile approximately fixed. The parameters (α_p, β_p) for the pressure profile given by Eq. (15) are (2.00,1.10).

No Mercier instability is observed with β_N ranging from 3.5 to 5.5. n=∞ ballooning instability occurred for $\beta_N > 4.5$ at the traditional location for reverse shear plasmas, where the magnetic shear begins to rise outside the q_{min} location.

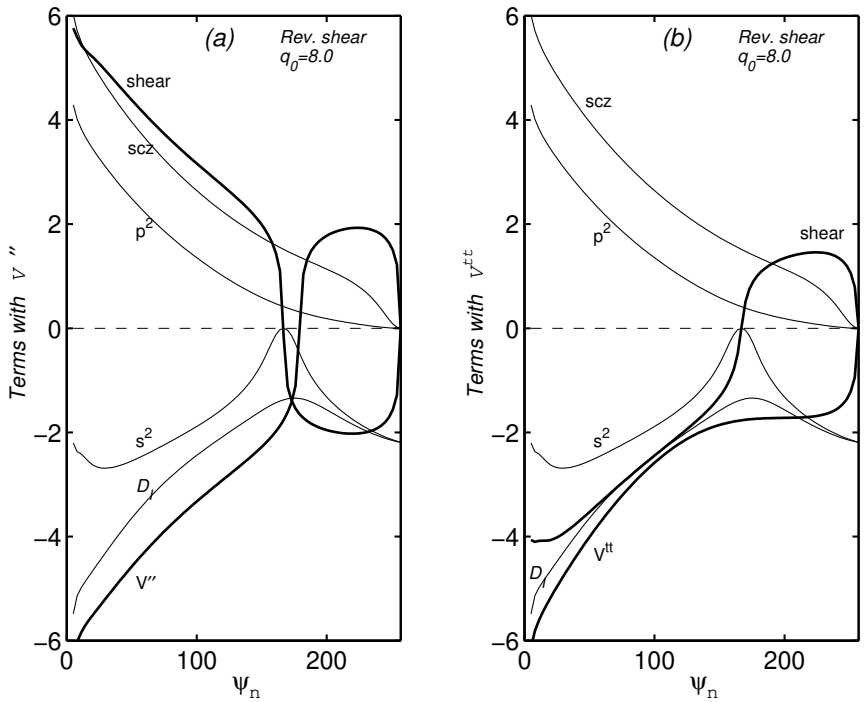

Figure 4: The terms of D_I using V'' (a), and V^{tt} (b), for a reversed shear profile. $q_{\rm axis} = 8.0$.

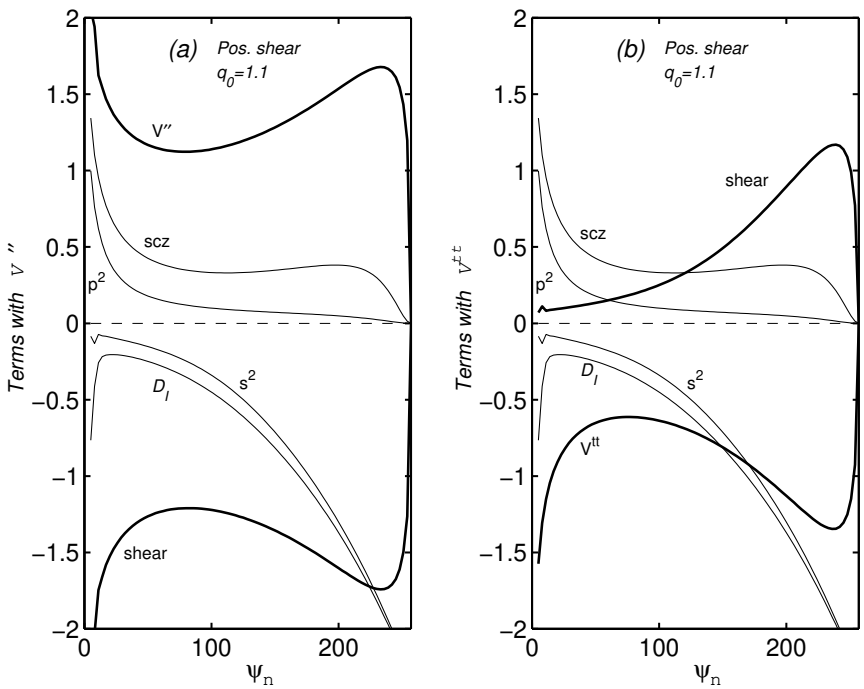

Figure 5: The terms of D_I using V'' (a), and V^{tt} (b), for a monotonic shear profile. $q_{\rm axis} = 1.1$.

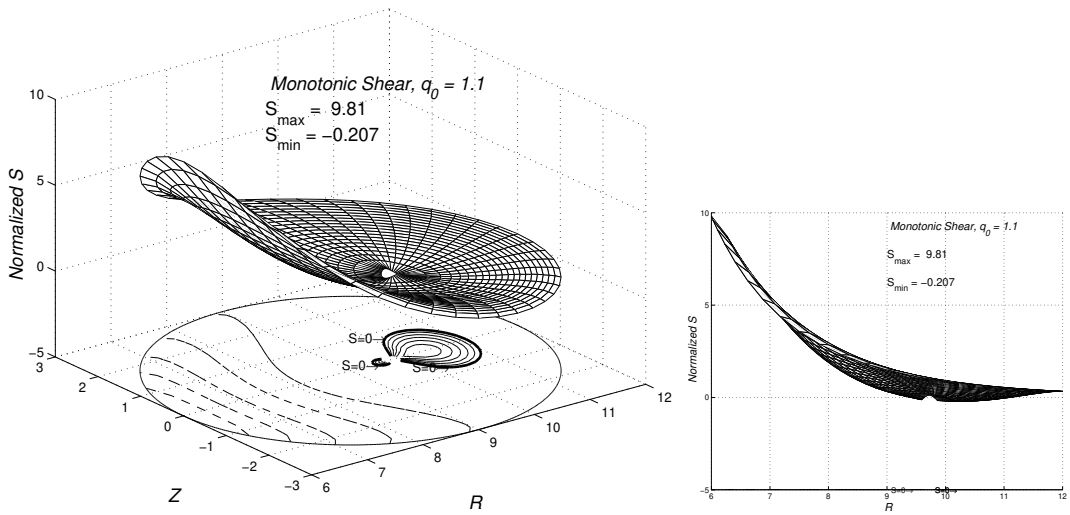

Figure 6: Two views of the contours of the normalized local shear on the R-Z plane together with a 3D display for a monotonic q profile for which $q_{\text{axis}} = 1.1$. Seven contour levels each for positive and negative $\hat{S}$ are shown. Dotted lines signify $\hat{S} \geq 0$, solid lines $\hat{S} \leq 0$, and the heavy solid lines, $\hat{S} = 0$, which are labeled. The mesh in the 3D figure is the computational grid in (ψ, θ). Most of the shear resides in the region of favorable curvature. The outermost circle is the plasma boundary.

In conclusion, no Mercier instability is observed for the ITER reversed shear plasma when q-axis is increased from the reference value, for a peaked pressure profile.

5 Local magnetic shear

The local magnetic shear, $S(\psi, \theta)$, defined in Sec. 2, plays an important role in the stability properties of plasmas. The significant differences in S between reversed and non-reversed shear plasmas which are illustrated here provide evidence that the reversed shear configurations examined are less susceptible to interchanges.

The intrinsic outward shift of the magnetic axis in tokamak configurations redistributes the poloidal flux so as to reduce the local magnetic shear at the outer major radius side. This opposition to imposed positive global shear in conventional non-reversed configurations results in a low shear neighborhood about a null in the local shear near the magnetic axis.

In Fig. 6 is plotted contours of $\hat{S}(\psi, \theta)$ for the non-reversed shear case. Seven equally distributed contour levels each for positive and negative $\hat{S}$ are shown. The vertical axis represents the contour values. Examination of the density of the lines shows that the local shear is negative (solid lines) out to about $R = 11$ and is very small and positive in the region of unfavorable curvature. This lack of shear tends to breed interchanges and but is compensated for by other effects. In reversed shear plasmas, on the other hand, the imposed negative global shear enhances the negative local shear tendency and render the plasma more stable in the reversed region by strengthening the (negative) shear and expanding the radial extent of the negative shear region. The null moves out towards the plasma edge where the pressure gradient is small. See Fig. 7. Ballooning modes are found to be least stable near the edge of reversed shear plasmas where the local shear is small. A fully reversed shear profile would cause the null to migrate beyond the plasma edge. In both cases it is an unfortunate trade off that most of the shear resides in the region of favorable curvature.

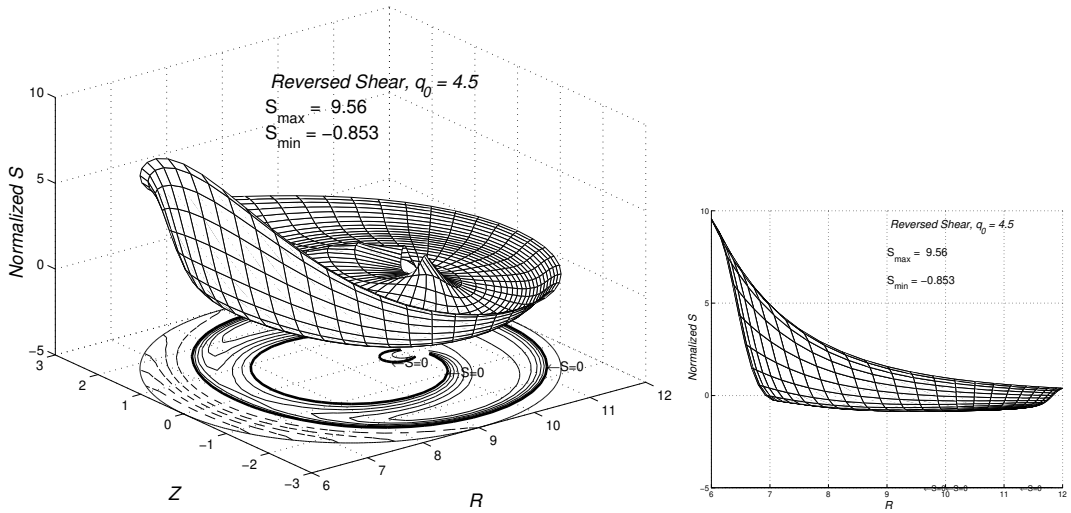

Figure 7: As in Fig. 6, two views of the contours of the normalized local shear for a reversed shear profile for which $q_{\rm axis} = 4.5$.

Note that $\hat{S}$ ranges from only -0.207 to 9.81 in the monotonic case and from -0.853 to 9.56 in the reversed shear case. This phenomenon where the axis shift provides sufficient (negative) shear is responsible, for example, for the second stability access to ballooning modes in bean shaped tokamaks where the shift imposed by the shaping is present even at low beta.[12]

Although these arguments involving the poloidal dependencies are more relevant to ballooning modes, they are pertinent to interchanges as well since the physical mechanisms of the instability are similar and furthermore ballooning stability is a sufficient condition for achieving interchange stability.

6 Reasons for the discrepancy

Since our results are largely in disagreement with [1], we can speculate on possible reasons for the discrepancy between the results of that study and the present one.

There may be differences in the ways in which the equilibria are calculated. As described above, we use a fixed boundary code in which the shape of the plasma boundary is given and held fixed during the course of the studies, even at high β. A free boundary equilibrium code could introduce unwanted distortions of the plasma boundary. We have studied D-shaped cross sections and have found that with positive D the plasma remains stable, as expected; however, plasmas with negative D shapes can be unstable in the inner region.

In Ref. [1], the toroidal field function, $g(V)$, where, $B_\phi = g/R$, is written as (in the notation of Ref. [1])

$$g = 2\pi \frac{d\Phi}{dV} \langle R^2 \rangle, \tag{31}$$

where Φ is the toroidal flux. g enters in the "shear" term of the Mercier expression. The relation for g could be a typographic error and may not have been used in the calculations. At any rate the correct relation should be,

$$g = 2\pi \frac{d\Phi}{dV} \frac{1}{\langle 1/R^2 \rangle}. \tag{32}$$

This could introduce an error of $\sim (a/R)^2$ in the calculations and may contribute to the discrepancy.

We have found also that it is important to calculate the integrals over θ very accurately because of the complicated geometrical structure of advanced tokamak configurations and the cancellations of large terms involved in the Mercier criterion. As stated before we utilized the exceptionally high accuracy offered by the simple trapezoidal rule for periodic functions.

7 Conclusions

In this work we have attempted to clarify the role of magnetic shear in the pressure driven stability properties of reversed shear configurations. Our results which shows that these configurations are robustly stable provided that the safety factor remains above unity and the triangularity is positive, contradict the recent results of Ozeki, et al. [1]. A regrouping of the terms in the Mercier criterion demonstrates that the shear terms are actually stabilizing and supports conclusions of both the numerical analyses and the semi-analytic model of Ref. [5]. The local magnetic shear analyses suggest that reversed shear configurations have more favorable stability properties. Possible reasons for the contradiction could be distortion of the equilibrium surfaces, errors in the analysis and inaccuracies in the numerical algorithms.

8 Acknowledgments

We have benefited from discussions with Dr. J. M. Greene and also from communications with Dr. T. Ozeki. Thanks are also due to F. W. Perkins and W. M. Tang for their encouragement throughout this study. Assistance from Dr. Stephan Brunner in the use of the *MATLAB* graphics package for the figures is gratefully acknowledged. This work was supported by U.S. Department of Energy Contract No. DE-AC02-76-CHO-3073.

References

[1] T. Ozeki, M. Azumi, S. Ishida, and T. Fujita. Violation of the Mercier criterion in reversed shear confinement configurations in tokamaks. *Plasma Physics and Controlled Fusion*, 40(6):871–877, June 1998.

[2] C. Mercier. Un critère nécessaire de stabilité hydromagnétique pour un plasma en symétrie de révolution. *Nuclear Fusion*, 1:47–53, 1960.

[3] C. Mercier. *The Magnetohydrodynamic Approach to the problem of Plasma Confinement in closed Magnetic Configurations*. Commission of the European Communities, Luxembourg, 1974.

[4] J. M. Greene and J. L. Johnson. Interchange instabilities in ideal hydromagnetic theory. *Plasma Physics*, 10(8):729–745, August 1968.

[5] J. M. Greene and M. S. Chance. The second region of stability against ballooning modes. *Nuclear Fusion*, 21(4):453–464, April 1981.

[6] Y. Nakamura, M. Wakatani, M. Furukawa, and K. Ichiguchi. Ideal and resistive interchange instabilities in negative shear tokamak and currentless heliotron plasmas. In IAEA, editor, *Seventeenth International Conference on Fusion Energy*, volume (to be published), page (to be published), Yokohama, Japan, October 1998. International Atomic Energy Agency, Vienna, International Atomic Energy Agency.

[7] J. Manickam, E. D. Fredrickson, Z. Chang, M. Okabayashi, et al. MHD studies in reversed shear plasma in TFTR. In IAEA, editor, *Sixteenth International Conference on Fusion Energy*, volume 1, pages 453–462, Montreal, October 1996. International Atomic Energy Agency, International Atomic Energy Agency.

[8] E. J. Strait, T. A. Casper, M. S. Chu, J. R. Ferron, et al. Stability of negative central magnetic shear discharges in the DIII-D tokamak. *Physics of Plasmas*, 4(5):1783–1791, May 1997.

[9] C. Kessel, J. Manickam, G. Rewoldt, and W. M. Tang. Improved plasma performance in tokamaks with negative magnetic shear. *Physical Review Letters*, 72(8):1212–1215, 1994.

[10] S. C. Jardin, C. E. Kessel, C. G. Bathke, D. A. Ehst, T. K. Mau, F. Najmabadi, T. W. Petrie, and the ARIES Team. Physics basis for a reversed shear tokamak power plant. *Fusion Engineering and Design*, 38:27–57, 1997.

[11] Germund Dahlquist and Åke Björck. *Numerical Methods*, chapter 7, pages 297–301. Prentice-Hall, inc., Englewood Cliffs, New Jersey, first edition, 1974.

[12] M. S. Chance, S. C. Jardin, and T. H. Stix. Balloooning mode stability of bean-shaped cross sections for high-β tokamak plasmas. *Physical Review Letters*, 51(21):1963–1966, November 1983.

[13] M. S. Chance, J. M. Greene, R. C. Grimm, and J. L. Johnson. Study of the MHD spectrum in an elliptic plasma column. *Nuclear Fusion*, 17(1):65–83, January 1977.

[14] W. A. Newcomb. Hydromagnetic stability of a diffuse linear pinch. *Annals of Physics*, 10:232–267, 1960.